INTEGRATED STRUCTURAL/TRIM OPTIMIZATION FOR ACTIVE AEROELASTIC WING TECHNOLOGY

P. Scott Zink*, Dimitri N. Mavris†, Daniella E. Raveh‡
Aerospace Systems Design Laboratory
School of Aerospace Engineering
Georgia Institute of Technology, Atlanta, GA 30332-0150

Abstract

A new process for concurrent trim and structural optimization of Active Aeroelastic Wing technology is presented. The new process treats trim optimization and structural optimization as integrated problems in the same mathematical formulation, in which control surface gear ratios are added as design variables to a standard structural optimization algorithm. This new approach is in contrast to most of the existing AAW design processes in which structural optimization and trim optimization are performed in an iterative, sequential manner. The new integrated AAW design process is demonstrated on a lightweight fighter type aircraft and compared to a sequential AAW design process. For this demonstration, the integrated process converges to a lower weight, and offers an advantage over the sequential process in that optimization is performed in one continuous run, whereas the sequential approach requires pausing and restarting the structural optimization to allow for trim optimization.

Introduction

An emerging and promising technology for addressing the problem of adverse aeroelastic deformation, such as control surface reversal, is Active Aeroelastic Wing (AAW) technology. It has recently been a key area of study for both the government and industry[1,2] and is defined by Pendleton et. al., as "a multidisciplinary, synergistic technology that integrates air vehicle aerodynamics, active controls, and structures together to maximize air vehicle performance"[3]. AAW technology exploits the use of leading and trailing edge control surfaces to aeroelastically shape the wing, with the resulting aerodynamic forces from the flexible wing becoming the primary means for generating control power. With AAW, the control surfaces then act mainly as tabs and not as the primary sources of control power as they do with a conventional control philosophy. As a result, wing flexibility is seen as an advantage rather than a detriment since the aircraft can be operated beyond reversal speeds and still generate the required control power for maneuvers. Hence, there is potential for significant reductions in structural weight and actuator power.

Figure 1 illustrates conceptually the differences between AAW technology and a conventional control approach. The hypothetical example shows the cross section of two wings deforming due to aeroelastic effects. The wing on the left employing AAW technology is twisting in a positive way with the use of both leading and trailing edge surfaces, while the conventionally controlled wing on the right, which uses only the trailing edge surface, is twisting in a negative way[4]. This adverse twist due to the deflection of the trailing edge surface is associated with reduced control surface effectiveness and control surface reversal, in which the increase in camber due to the deflection of the surface is offset by the negative twist of the wing[5].

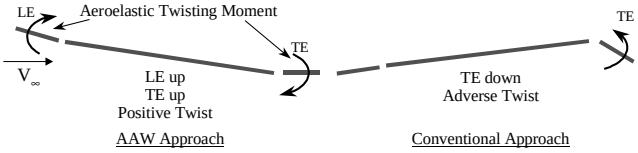

Figure 1 - AAW Technology vs. Conventional Control

Since AAW technology is multidisciplinary in nature, structural design using the technology necessarily requires detailed information about the vehicle structures, aerodynamics, and controls, and in particular, is heavily dependent on control law design. Thus, there is a need for an integrated AAW design process in which the structure and control laws are optimized concurrently.

In consideration of AAW technology's use of redundant control surfaces, an important constituent of the technology are *control surface gear ratios* which dictate how one control surface deflects with respect to a single basis surface. Two gear ratio scenarios are illustrated in Figure 2 in which the deflections of the leading edge inboard (LEI), leading edge outboard (LEO), and trailing edge inboard (TEI) surfaces are linearly dependent on the deflection of the trailing edge outboard surface (TEO). This concept is also referred

---

* Ph.D. Candidate, Student Member AIAA
† Boeing Chair in Advanced Aerospace Systems Analysis, Senior Member AIAA
‡ Postdoctoral Fellow, Member AIAA

to as control surface blending and for the purposes of this research constitute the control laws.

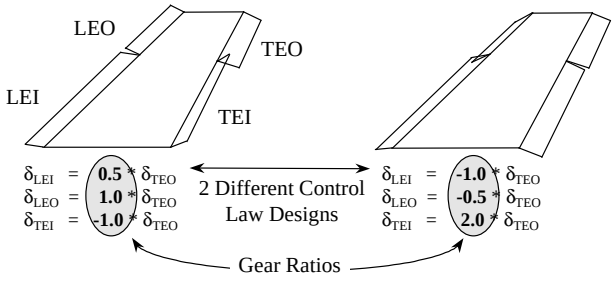

Figure 2 – Gear Ratio Illustration

The *AAW design process* refers to the concurrent optimization of the structure and gear ratios. Structural optimization refers to the sizing of structural elements (e.g., skin thickness, spar thickness) to minimum weight, subject to stress, aeroelastic constraints, etc. Trim optimization refers to the process of selecting the gear ratios, or control surface deflection angles, that trim the aircraft to a prescribed maneuver while minimizing loads within actuator limits. The need for trim optimization is due to AAW technology's use of redundant control surfaces, which means that the static aeroelastic trim equations cannot be solved in a closed form manner. Much research has been done in this area, where References [6], [7], [8], [9], and [10] discuss several approaches by which this problem has been tackled.

The literature dealing with the AAW design process is more limited, and most of the methods that have been developed are those in which trim optimization and structural optimization are performed sequentially. Zillmer[11,12] developed such an approach. In this case, trim optimization, performed using a Rockwell-developed code ISMD (Integrated Structure/Maneuver Design), is embedded in an iterative process with NASTRAN[13]. The maneuver loads due to the optimized deflections from ISMD are transferred to NASTRAN which then optimizes the structure to minimum weight. NASTRAN then passes stability derivatives and sensitivity information of the current structural design to ISMD for another trim optimization. This process repeats itself until the wing weight converges.

Another example, in the literature, of a sequential AAW design process is found in Love et al.[9] In this case, the trim optimization module, where the deflection of the control surfaces are optimized to minimize user-defined component loads (e.g. root bending moment, hinge moment), was placed within the structural optimization loop of ASTROS (Automated Structural Optimization System)[14], a finite element-based structural optimization code. For each iteration in the structural optimization, the control surface deflections for the current structural design are optimized. Then with these new deflections the structural optimizer proceeds to take another step, pauses again for trim optimization, and so on, until the structural optimization objective, wing weight, converges.

Zink et al.[15,16] applied the techniques of Reference [9] in a design study of a generic lightweight fighter concept employing AAW technology, with four wing control surfaces and a horizontal tail. Trim optimization was performed for antisymmetric (rolling) and symmetric maneuvers. The trim optimization problem for the symmetric maneuver was posed as a minimization of root bending moment (RBM), whereas a summation of the wing hinge moments was the objective for the antisymmetric maneuvers. It was solved using a gradient based optimization algorithm. The intention was that trim and structural optimization would be repeated iteratively. However, only the first step was demonstrated, as trim optimization was performed only once on the starting structural design. As an evolution of the work in References [15] and [16], and in addressing some of the problems encountered in that study, a new sequential AAW design process was developed that employs the simplex method[17] for trim optimization. This new sequential process is reviewed briefly in the current work and documented in detail in Reference [10].

Miller[6] proposed an AAW design process in which the thickness of structural elements and the control surface deflections were simultaneous design variables in an integrated optimization problem. However, it was implemented, evidently, with limited success, as Zillmer[11] reports that the original integrated algorithm was abandoned in lieu of the sequential algorithm discussed above.

In the current research, a similar AAW design process is developed in which trim and structural optimization are posed as an integrated problem in the same mathematical formulation. However, in this approach, the control surface gear ratios, rather than their deflections, are added as design variables to the structural optimization. Additionally, hinge moments are included in the optimization problem as constraints. The possible advantages of this integrated AAW design process include better solution convergence and lower weight structural designs. Its development and comparison with the sequential AAW design process of Reference [10] is the goal of the current effort.

Methodology

Integrated AAW Design Process

The formulation of the integrated AAW design process is as follows:

Minimize: *Weight*
Subject to: *Static Aeroelastic Constraints (Material strain allowables)*
Control Surface Travel Limits
$-30^o \le \delta_{LEI} \le 5^o$, $-30^o \le \delta_{LEO} \le 5^o$,
$-30^o \le \delta_{TEI} \le 30^o$, $-30^o \le \delta_{TEO} \le 30^o$,
$-30^o \le \delta_{HT} \le 30^o$
Hinge Moment Constraints
$-3.0*10^5 \le HM_{LEI} \le 3.0*10^5$,
$-1.0*10^5 \le HM_{LEO} \le 1.0*10^5$,
$-1.5*10^5 \le HM_{TEI} \le 1.5*10^5$,
$-5.0*10^4 \le HM_{TEO} \le 5.0*10^4$ (lb-in)

Design Variables:
$t_1,\ldots t_n$, $g_1,\ldots g_m$
n: number of thickness variables
m: number of gear ratio design variables

where t_i are the traditional structural design variables, g_i are the new gear ratio design variables, HT is the horizontal tail, HM_i are the control surface hinge moments, and δ_i are the control surface deflections. The control surface travel limits and hinge moment limits are based on typical allowables for modern fighter aircraft.

The optimization problem above is implemented in modal-based ASTROS, which provides efficient and accurate finite element-based static aeroelastic analysis and optimization[18,19]. The optimization problem is solved by the Modified Method of Feasible Directions[20] algorithm. At the heart of the modal approach is the representation of the discrete displacements as a linear combination of the free aircraft low frequency modes of vibration which are then used to create generalized stiffness, mass, and force matrices for the static aeroelastic equation. As a result, the size of the analysis and optimization problem is significantly reduced.

Although the optimal weight is not an explicit function of the gear ratios, the stress/strain, and hinge moment constraints are, and thus sensitivities of these constraints with respect to each of the gear ratios of interest for each maneuver are required. Analytical sensitivities of these constraints have been derived for the static aeroelastic equation in modal coordinates. The sensitivities of the objective and constraints with respect to the thickness variables are provided in Reference [21] and will not be repeated here.

Gear Ratio Sensitivities

The basic equation for static aeroelastic analysis in discrete coordinates is[22]:

$$[[K] - q[AICS]]\{u\} + [M][\phi_r]\{\ddot{u}_r\} = [P]\{\delta\} \tag{1}$$

where [K] is the stiffness matrix, [AICS] is the aerodynamic influence coefficients matrix transformed to the structural degrees of freedom, {u} are the displacements and rotations at the structural nodes, [M] is the mass matrix, $[\phi_r]$ are the rigid body modes of the free aircraft, $\{\ddot{u}_r\}$ is a vector of rigid body accelerations, [P] is a matrix of the rigid aerodynamic force coefficients due to aerodynamic trim parameters, q is the dynamic pressure, and {δ} is the aerodynamic trim parameter values (e.g., angle of attack, control surface deflection, roll rate).

Equation (1) is transformed to modal coordinates by assuming that the displacements, {u}, are a linear combination of the low frequency modes of vibration, as given by:

$$\{u\} = [\phi_r \quad \phi_e]\begin{Bmatrix}\xi_r \\ \xi_e\end{Bmatrix} \tag{2}$$

where $[\phi_r \quad \phi_e]$ is the modal matrix comprised of the rigid body modes, $[\phi_r]$, and a subset of the elastic modes, $[\phi_e]$. $\{\xi_r\}$ are the rigid body modal displacements, and $\{\xi_e\}$ are the elastic modal displacements. Substitution of Equation (2) into Equation (1) and pre-multiplication of Equation (1) by the transpose of the modal matrix yields the static aeroelastic equation in modal coordinates[21]:

$$\begin{bmatrix} -qGAIC_{rr} & -qGAIC_{re} \\ -qGAIC_{er} & GK_{ee} - qGAIC_{ee}\end{bmatrix}\begin{Bmatrix}\xi_r \\ \xi_e\end{Bmatrix} + \begin{bmatrix} M_{rr} \\ M_{er}\end{bmatrix}\{\ddot{\xi}_r\} = \begin{bmatrix} PA_r \\ PA_e\end{bmatrix}\{\delta\} \tag{3}$$

Considering that with AAW technology {δ} contains a redundant number of aerodynamic trim parameters, a gearing matrix ($\{\delta\} = [G]\{\delta_1\}$) is introduced to the right hand side of Equation (3). This gearing matrix, [G], contains the gear ratios, g_i, and relates the redundant (dependent) trim parameters to the determinate (independent) ones, $\{\delta_1\}$. Taking the derivative of Equation (3) (where [GPA] = [PA][G]) with respect to the i^{th} gear ratio results in the following:

$$\begin{bmatrix} -qGAIC_{rr} & -qGAIC_{re} \\ -qGAIC_{er} & GK_{ee} - qGAIC_{ee} \end{bmatrix} \begin{Bmatrix} DXIG_r \\ DXIG_e \end{Bmatrix}_i + \begin{bmatrix} M_{rr} \\ M_{er} \end{bmatrix} \{DUDG_r\}_i = \begin{bmatrix} GPA_r \\ GPA_e \end{bmatrix} \{DDELG\}_i + \begin{bmatrix} DGPAG_r \\ DGPAG_e \end{bmatrix}_i \{\delta_1\} \quad (4)$$

where:

$$\{DXIG_r\}_i = \frac{\partial\{\xi_r\}}{\partial g_i} \qquad \{DXIG_e\}_i = \frac{\partial\{\xi_e\}}{\partial g_i}$$

$$\{DUDG_r\}_i = \frac{\partial\{\ddot{\xi}_r\}}{\partial g_i} \qquad \{DDELG\}_i = \frac{\partial\{\delta_1\}}{\partial g_i}$$

$$[DGPAG_r]_i = \frac{\partial[GPA_r]}{\partial g_i} \quad [DGPAG_e]_i = \frac{\partial[GPA_e]}{\partial g_i}$$

Combining the left hand terms of Equation (4):

$$\begin{bmatrix} -qGAIC_{rr} & -qGAIC_{re} & M_{rr} \\ -qGAIC_{er} & GK_{ee} - qGAIC_{ee} & M_{er} \end{bmatrix} \begin{Bmatrix} DXIG_r \\ DXIG_e \\ DUDG_r \end{Bmatrix}_i = \begin{bmatrix} GPA_r \\ GPA_e \end{bmatrix} \{DDELG\}_i + \begin{bmatrix} DGPAG_r \\ DGPAG_e \end{bmatrix}_i \{\delta_1\} \quad (5)$$

Equation (5) is a system of $n_r + n_e$ equations with $2n_r + n_e$ unknown sensitivities (n_r and n_e is the number of rigid body modes and elastic modes respectively, $\{\delta_1\}$ is known as we are differentiating about a known static aeroelastic equilibrium condition). For example, if the rigid body accelerations, $\{\ddot{\xi}_r\}$, are defined by the user for a specific maneuver, then $\{DUDG_r\}_i$ is zero, since the accelerations are constant. In this case, then, the unknown sensitivities are $\{DXIG_e\}_i$, $\{DXIG_r\}_i$, and $\{DDELG\}_i$, which are more unknowns than equations available to solve them. As a result, an additional equation is introduced which is based on the assumption that the displacement, $\{u\}$, does not change the location of the center of gravity or orientation of the mean axis system, which defines the alignment of the aircraft moments of inertia[23]. This assumption leads to the rigid body modes, $[\phi_r]$, being orthogonal to the displacement vector, $\{u\}$, with respect to the mass matrix, which expressed in modal coordinates leads to the following equation:

$$[M_{rr}]\{\xi_r\} + [M_{er}]^T \{\xi_e\} = \{0\} \quad (6)$$

Differentiating with respect to g_i, Equation (6) becomes:

$$[M_{rr}]\{DXIG_r\}_i + [M_{er}]^T \{DXIG_e\}_i = \{0\} \quad (7)$$

Solving for $\{DXIG_r\}_i$:

$$\{DXIG_r\}_i = -[M_{rr}]^{-1}[M_{er}]^T \{DXIG_e\}_i \quad (8)$$

Substituting Equation (8) into Equation (5), Equation (5) becomes:

$$\begin{bmatrix} q[GAIC_{rr}][M_{rr}]^{-1}[M_{er}]^T - q[GAIC_{re}] & [M_{rr}] \\ q[GAIC_{er}][M_{rr}]^{-1}[M_{er}]^T + [GK_{ee}] - q[GAIC_{ee}] & [M_{er}] \end{bmatrix} \times \begin{Bmatrix} DXIG_e \\ DUDG_r \end{Bmatrix}_i = \begin{bmatrix} GPA_r \\ GPA_e \end{bmatrix} \{DDELG\}_i + \begin{bmatrix} DGPAG_r \\ DGPAG_e \end{bmatrix}_i \{\delta_1\} \quad (9)$$

Taking the 2nd row of Equation (9) and solving for $\{DXIG_e\}_i$:

$$\{DXIG_e\}_i = [GKA_{ee}]^{-1} \left(\begin{matrix} [GPA_e]\{DDELG\}_i - \\ [M_{er}]\{DUDG_r\}_i + \\ [DGPAG_e]_i \{\delta_1\} \end{matrix} \right) \quad (10)$$

where:

$$[GKA_{ee}] = q[GAIC_{er}][M_{rr}]^{-1}[M_{er}]^T + [GK_{ee}] - q[GAIC_{ee}] \quad (11)$$

Substituting Equation (10) into the 1st row of Equation (9), and rearranging terms, the first row of Equation (9) can be written as:

$$[LHSA]\{DUDG_r\}_i = [RHSA]\{DDELG\}_i + [DRHSG]_i \{\delta_1\} \quad (12)$$

where:

$$[LHSA] = [M_{rr}] + q[GAIB_{re}][GKA_{ee}]^{-1}[M_{er}] \quad (13)$$

$$[RHSA] = [GPA_r] + q[GAIB_{re}][GKA_{ee}]^{-1}[GPA_e] \quad (14)$$

$$[DRHSG]_i = [DGPAG_r]_i + q[GAIB_{re}][GKA_{ee}]^{-1}[DGPAG_e]_i \quad (15)$$

$$[GAIB_{re}] = [GAIC_{re}] - [GAIC_{rr}][M_{rr}]^{-1}[M_{er}]^T \quad (16)$$

Equation (12) is used to solve for the n_r unknown trim *sensitivities*. These sensitivities are calculated through algebraic manipulation of Equation (12), and are substituted into Equation (10) to find the elastic modal displacement sensitivities, $\{DXIG_e\}_i$. The rigid modal displacement sensitivities $\{DXIG_r\}_i$ are then estimated by substitution of $\{DXIG_e\}_i$ into Equation (8). Once the sensitivities for the modal displacements are found, the sensitivities for stress and strain can be easily calculated by multiplying the modal displacement sensitivities by the fixed strain-displacement, stress-displacement relationships.

Sensitivities of Aerodynamic Loads to Gear Ratios

The total aerodynamic loads (including those due to flexibility effects) on the aerodynamic grid is[21]:

$$\{P_k\} = q\begin{pmatrix}[AIRFRC]\{\delta_1\}+\\ [AIC]\left([GGS_{ke}]\{\xi_e\}+[GGS_{kr}]\{\xi_r\}\right)\end{pmatrix} \quad (17)$$

Differentiating Equation (17) with respect to g_i, Equation (17) becomes:

$$\{DPKG\}_i = q\begin{pmatrix}[AIRFRC]\{DDELG\}_i+\\ [DAIRFRCG]_i\{\delta_1\}+\\ [AIC]\left([GGS_{ke}]\{DXIG_e\}_i+\\ [GGS_{kr}]\{DXIG_r\}_i\right)\end{pmatrix} \quad (18)$$

where $\{DDELG\}_i$, $\{DXIG_e\}_i$, $\{DXIG_r\}_i$ are defined previously, [AIRFRC] are the rigid aerodynamic force coefficients in the aerodynamic degrees of freedom, $[GGS_{ke}]$ and $[GGS_{kr}]$ are spline matrices transforming displacements in modal coordinates to displacements in the aerodynamic grid, and:

$$\{DPKG\}_i = \frac{\partial\{P_k\}}{\partial g_i} \qquad [DAIRFRCG]_i = \frac{\partial[AIRFRC]}{\partial g_i}$$

The sensitivities of the hinge moment constraints can then be found by multiplying $\{DPKG\}_i$ by an appropriate transformation matrix which represents the moment arm and remains fixed throughout the optimization. The analytical sensitivities presented here and in the previous subsection have been verified by comparing them with sensitivities estimated by numerical differentiation. (using finite differences). The agreement between the analytical and numerical sensitivities is quite good.

Sequential AAW Design Process

The sequential AAW design process of Reference [10] is performed by iterating between trim optimization, by the simplex method in Matlab[24], and structural optimization by modal-based ASTROS, as presented in Figure 3. For each structural optimization iteration, the control surface deflections for the current structural design are optimized. Then, these new control surface deflections are converted to gear ratios and passed to the structural optimizer, which then proceeds to take another step. After the structural optimization step, the aeroelastic equations for the new structural design are assembled, and the appropriate stability derivatives, trim objective and constraint coefficients are calculated in ASTROS and then output to trim optimization. This process repeats itself until the structural optimization objective, wing weight, is converged.

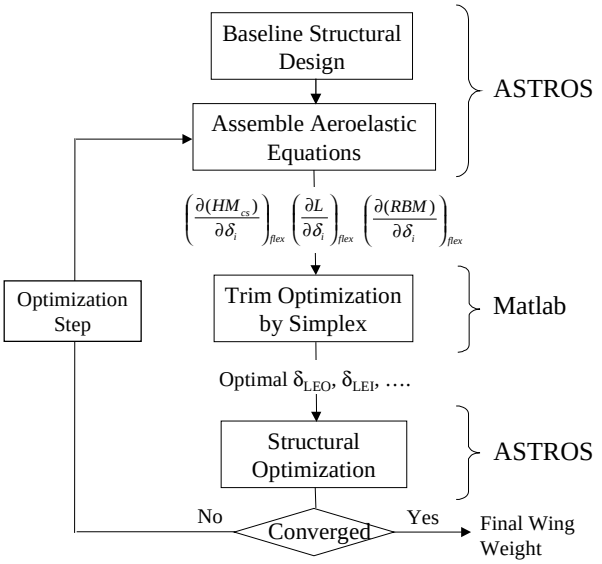

Figure 3 – Sequential AAW Design Process[10]

Trim optimization, for the symmetric maneuvers of Reference [10], is posed as a minimization of root bending moment (RBM), where the wing control surfaces are used to tailor the load distribution and provide load relief at the wing root, thus ultimately reducing wing weight.

The symmetric trim optimization problem[10] is formally stated as:

Minimize:

$$RBM = \sum_{i=1}^{n_{cs}}\left(\frac{\partial(RBM)}{\partial\delta_i}\right)_{flex}\delta_i + \left(\frac{\partial(RBM)}{\partial\alpha}\right)_{flex}\alpha \quad (19)$$

Subject to: *Control Surface Travel Limits*
Hinge Moment (HM) Constraints

where the hinge moment for each control surface (cs) is given by:

$$HM_{cs} = \sum_{i=1}^{n_{cs}} \left(\frac{\partial (HM_{cs})}{\partial \delta_i} \right)_{flex} \delta_i + \left(\frac{\partial (HM_{cs})}{\partial \alpha} \right)_{flex} \alpha + \left(\frac{\partial (HM_{cs})}{\partial a_z} \right)_{flex} a_z \quad (20)$$

Satisfaction of Trim Equations (Lift and Pitching Moment Balance)

$$\sum_{i=1}^{n_{cs}} \left(\frac{\partial L}{\partial \delta_i} \right)_{flex} \delta_i + \left(\frac{\partial L}{\partial \alpha} \right)_{flex} \alpha + L_{const} = ma_z \quad (21)$$

$$\sum_{i=1}^{n_{cs}} \left(\frac{\partial M}{\partial \delta_i} \right)_{flex} \delta_i + \left(\frac{\partial M}{\partial \alpha} \right)_{flex} \alpha + M_{const} = 0 \quad (22)$$

Design Variables: α, δ_{LEI}, δ_{LEO}, δ_{TEI}, δ_{TEO}, δ_{HT}

where α is the angle of attack, a_z is the vertical acceleration, m is the aircraft mass, n_{cs} is the number of control surfaces, and L_{const} and M_{const} refer to the lift and moment terms that are not dependent on control surface deflection and angle of attack. The lift and moment derivatives of Equations (21) and (22) are the dimensional flexible stability derivatives, and are estimated by solution of the static aeroelastic equation, Equation (1). Similarly, the flexible component load derivatives (∂(RBM)/$\partial\delta$, ∂(HM)/$\partial\delta$) are estimated by multiplying the applied loads (both inertial and aeroelastic) due to a unit deflection of the trim parameter, by an appropriate matrix that represents the moment arm from each grid point to the section about which the moment is being calculated. The control surface travel limits and hinge moment limits are the same as those for the integrated AAW design process, to allow for a fair comparison of both AAW design processes.

For the antisymmetric maneuvers, trim optimization in the sequential approach is formulated as a minimization of the total hinge moments, subject to the surface travel limits, hinge moment constraints, and trim balance requirements, as given formally by:

Minimize: $|HM_{LEI}| + |HM_{LEO}| + |HM_{TEI}| + |HM_{TEO}|$
Subject to: *Control Surface Travel Limits*
Hinge Moment Constraints
where the hinge moment for each control surface is:

$$HM_{cs} = \sum_{i=1}^{n_{cs}} \left(\frac{\partial (HM_{cs})}{\partial \delta_i} \right)_{flex} \delta_i + \left(\frac{\partial (HM_{cs})}{\partial p} \right)_{flex} p \quad (23)$$

Satisfaction of Trim Equations (Roll Moment Balance)

$$\sum_{i=1}^{n_{cs}} \left(\frac{\partial £}{\partial \delta_i} \right)_{flex} \delta_i + \left(\frac{\partial £}{\partial p} \right)_{flex} p = 0 \quad (24)$$

Design Variables: δ_{LEI}, δ_{LEO}, δ_{TEI}, δ_{TEO}

where £ is rolling moment, and p is the user-specified roll rate. Again, the coefficients of Equations (23) and (24) are obtained from a static aeroelastic analysis in modal-based ASTROS.

Numerical Example

Structural and Aerodynamic Model

The structural model of the aircraft used both in this research and in Reference [10] is shown in Figure 4. It is an ASTROS preliminary design finite element model of a lightweight composite fighter aircraft with 4 wing control surfaces (2 trailing edge, 2 leading edge) and a horizontal tail[18,25]. It corresponds to a wing with an aspect ratio of 3.0, a total planform area of 330 ft^2, a taper ratio of 20.0%, a leading edge sweep of 38.7°, and a thickness ratio of 3%. The skin of the wing is made up of 4 composite plies with orientations of 0°, ± 45°, and 90°, where the thickness of the –45° and +45° plies are constrained to be equal.

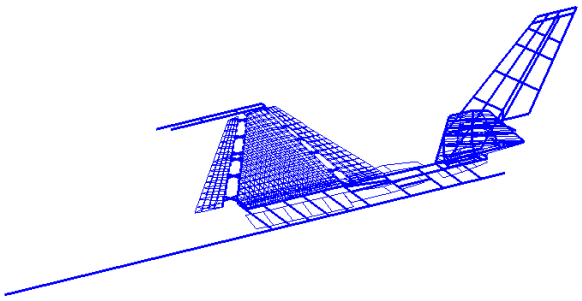

Figure 4 - Structural Model of Generic Fighter

The aerodynamic model is shown in Figure 5. It is a flat-panel Carmichael[26] model containing 143 vertical panels and 255 horizontal panels. It also contains paneling for the four wing control surfaces and horizontal tail to coincide with the control surfaces on the structural model. Carmichael aerodynamic influence coefficients are produced for two Mach numbers, 0.95 and 1.2, for both symmetric and antisymmetric conditions[27].

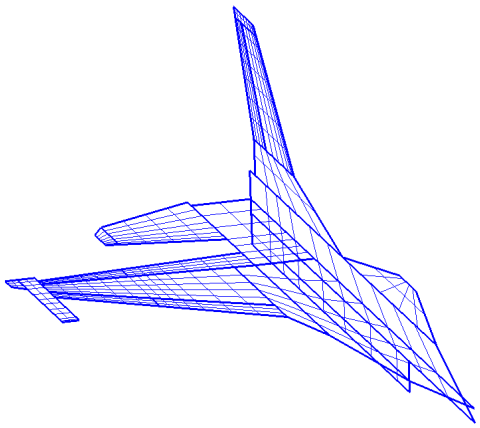

Figure 5- Aerodynamic Model of Generic Fighter

The structural design variables (t_i) in the AAW design process are the layer thickness of the composite skins. The number of structural design variables is 78 due to physical linking of the skin elements. Internal structure and carry-through structure remain fixed. Table 1 shows the maneuver conditions and strength constraints to which the structure is designed for both the sequential and integrated AAW design processes. Of course, for the integrated approach, hinge moment constraints and control surface travel limits are also included, as discussed in a previous section.

Table 1 - Maneuver Conditions and Design Constraints

Maneuver Condition	Design Constraint
1) Mach 0.95, 10,000 ft. 9g Pull Up	fiber strain: 3000 με tension 2800 με compression
2) Mach 1.20, Sea Level -3g Push Over	fiber strain: 3000 με tension 2800 με compression
3) Mach 1.20, Sea Level Steady State Roll = 100^O/s	fiber strain: 1000 με tension 900 με compression
4) Mach 0.95, 10,000 ft. Steady State Roll = 180^O/s	fiber strain: 1000 με tension 900 με compression

The gear ratio design variables (g_i) of the integrated process, for each maneuver, are shown in Table 2, along with the independent surface for each maneuver to which the dependent surfaces are geared. For example, the variable, g_{LEI3}, is the ratio of the deflection of the LEI surface to the deflection of the LEO surface for the supersonic roll.

Table 2 – Gear Ratio Design Variables

	Independent Surface	Gear Ratio Design Variables
Maneuver 1	HT	g_{LEI1}, g_{LEO1}, g_{TEI1}, g_{TEO1}
Maneuver 2	HT	g_{LEI2}, g_{LEO2}, g_{TEI2}, g_{TEO2}
Maneuver 3	LEO	g_{LEI3}, g_{TEI3}, g_{TEO3}
Maneuver 4	TEO	g_{LEI4}, g_{LEO4}, g_{TEI4}

Results

The integrated AAW design process here proposed has been implemented in modal-based ASTROS and demonstrated on the previously discussed model. It has been compared with the sequential AAW design process, discussed in detail in Reference [10]. As shown in Table 3, a comparison of the optimal weights by each approach reveals that the integrated approach converges to a slightly lower weight. In both cases, the number of iterations to reach the final solution was seven, indicating similar convergence rates between the two approaches.

Table 3 – Final Weights for each AAW Design Process

AAW Design Process	Weight (lb)
Sequential	292.3
Integrated	278.5

The integrated process was found to be sensitive to the gear ratio starting values. This may be a result of a limitation that exists in the integrated process as it is currently implemented in ASTROS. The limitation is that the deflection angles of the dependent control surfaces are unable to be directly constrained. To avoid unrealistic control surface deflections, separate constraints were applied to the independent control surface and the gear ratios. This limitation will be removed in future refinements of the integrated design process. For the current process, it has been found that the best starting gear ratios were those based on the starting control surface deflections for the sequential approach. In other words, the optimal deflections of trim optimization on the starting structural design provide a good point from which to start the integrated approach. The one exception to this are the starting gear ratios for the subsonic roll (Maneuver 4) in which a starting point different than that for the sequential approach was used.

Table 4 presents the final gear ratios for the subsonic pull-up by both the sequential and integrated AAW design processes. Both scenarios are quite similar, with both methods using heavily the outboard surfaces in a negative manner. Unlike for a conventional control approach, in this case, the horizontal tail is deflecting positively while the trailing edge surfaces are deflecting negatively to provide the

required pitching moment for trim. The leading edge control surfaces are also deflecting negatively for load alleviation. As a result of the heavy negative deflection of the outboard surfaces the center of pressure is shifted inboard, thus relieving load at the wing root. However the two approaches differ somewhat in their use of the inboard surfaces with the integrated approach using the TEI surface very little and the LEI surface rather heavily. This point is further illustrated in Figure 6 which is a history of the gear ratios over the course of both design approaches. Although it starts at the same point, the integrated approach very quickly diverges from the sequential in its use of the inboard surfaces.

Table 4 – Final Gear Ratios for Subsonic Pull-Up

	Sequential	Integrated
g_{LEI1}	-5.903	-10.098
g_{LEO1}	-38.575	-40.000
g_{TEI1}	-8.337	-0.722
g_{TEO1}	-38.575	-39.974

tends to relieve load at the root, and thus ultimately reduce weight. The authors found that the supersonic push-over is not a particularly critical maneuver that drives the design. Hence, in the integrated approach, gear ratios associated with this maneuver move very little from their starting values.

Table 5 - Final Gear Ratios for Supersonic Push-Over

	Sequential	Integrated
g_{LEI2}	1.855	1.584
g_{LEO2}	1.855	1.781
g_{TEI2}	-10.872	-10.005
g_{TEO2}	5.748	4.733

Table 6 shows the final gear ratios for the supersonic roll. In this case the LEO surface is the independent surface to which the others are geared, and it deflects in a positive manner (nose-up) to produce positive roll moment. The integrated approach favors heavier usage of all of the control surfaces relative to the LEO surface as indicated by the higher gear ratios.

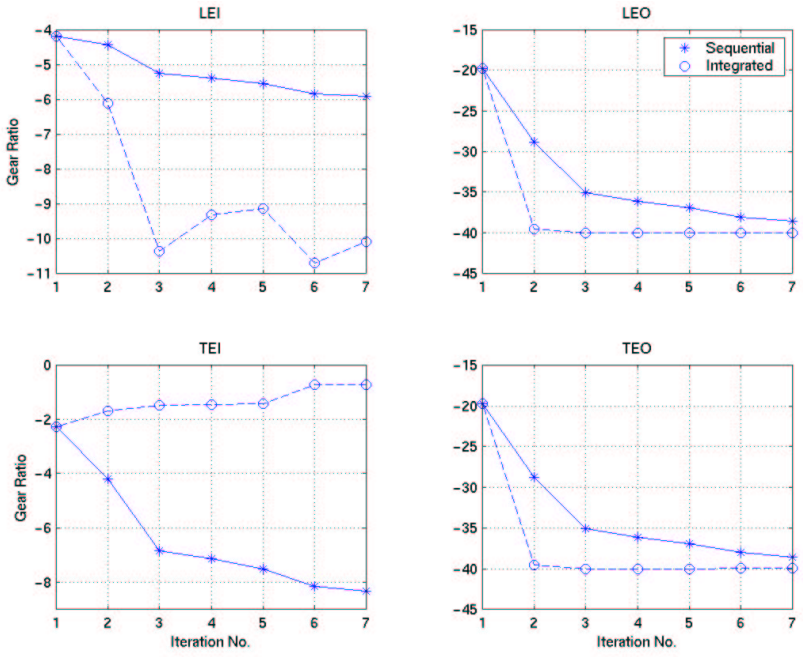

Figure 6 - Gear Ratio History (Maneuver 1)

The final gear ratios for the supersonic push-over are shown in Table 5. In this case both approaches produce very similar results in which the leading edge surfaces deflect positively. This is exactly the opposite trend of the subsonic pull-up, and is due to the fact that Maneuver 2 is a push-over maneuver, where the bending moments at the root are naturally negative. As a result, positive deflection of the leading edge surfaces This difference can likely be attributed to the different objectives of the two approaches. While the hinge moments are the trim optimization objective of the sequential approach, in the integrated approach, they are not part of the objective (although their values are constrained). Consequently, in the integrated approach, the gear ratios are used to relieve strains, so that the structural weight can be driven even lower.

Table 6 - Final Gear Ratios for Supersonic Roll

	Sequential	Integrated
g_{LEI3}	0.149	0.467
g_{TEI3}	0.007	0.023
g_{TEO3}	0.230	0.742

Table 7 - Final Gear Ratios for Subsonic Roll

	Sequential	Integrated
g_{LEI4}	0.206	0.400
g_{LEO4}	0.327	0.400
g_{TEI4}	-0.156	1.257

Finally, Table 7 contains the final gear ratios for the subsonic roll. In this case the TEO surface is the independent surface, since at subsonic Mach numbers it is still an effective surface. This is the one maneuver where the starting gear ratios for the integrated approach are not the same as those for the sequential approach. Whereas the sequential approach favors a negative gear ratio for the TEI surface, the authors found that the integrated approach favors a positive gear ratio for the TEI surface. This was discovered when the starting value for g_{TEI4} was selected to be positive. Over the course of the optimization by the integrated approach g_{TEI4} continues to get more positive as shown in Figure 7.

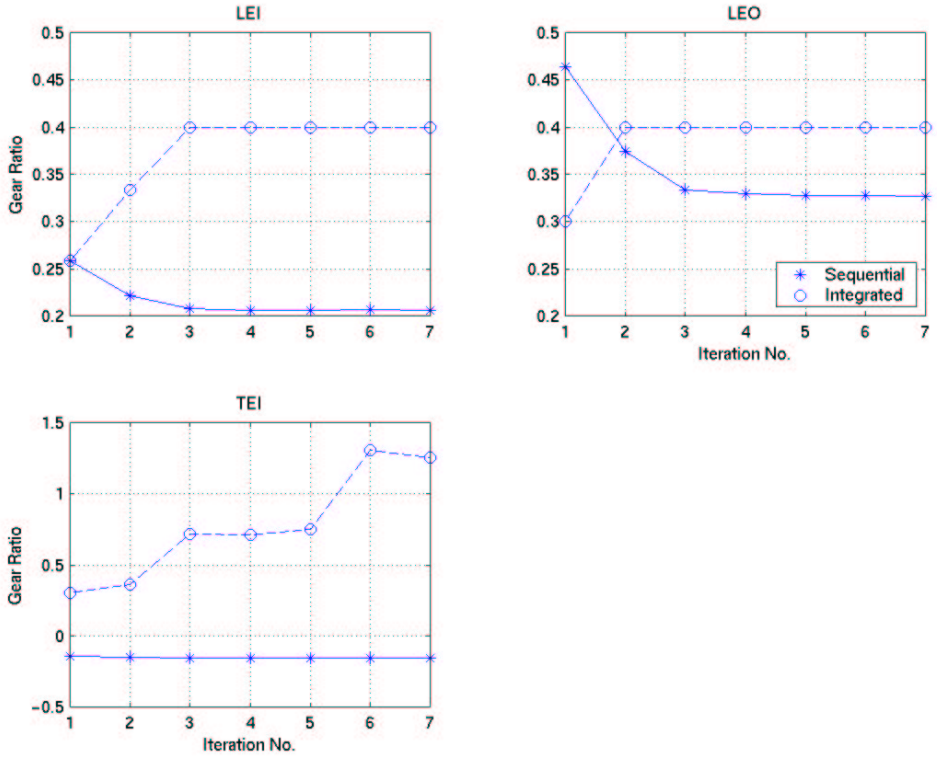

Figure 7 - Gear Ratio History (Maneuver 4)

For the studied test case, the optimal weight by the integrated approach was 5% less than that of the sequential approach. Based on this small difference it cannot be concluded that the integrated approach results in a lighter structural design in all cases. However, it is the notion of the authors that greater weight reduction can be demonstrated with the integrated approach once the current limitations that were previously discussed are removed. Moreover, since the integrated approach drives the element strains to lower values, it is expected that greater weight reduction can be achieved when structural elements other than the skins are designed.

The integrated approach holds much promise and has the one distinct advantage of not relying on a separate trim optimization being performed for every structural iteration. In addition, it does not require the creation of a separate objective for trim optimization (as does the sequential approach) that may not contribute to a maximal reduction in weight. For example, with the

antisymmetric maneuvers, the trim optimization objective for the sequential approach is the summation of all hinge moments. The control surfaces are deflected to minimize this objective, and then these deflections are passed to structural optimization. However, there is no guarantee that the control surface deflections are those that minimize weight. Perhaps there is a trim optimization objective that would produce deflections that would reduce the weight even further.

Conclusion

A new integrated AAW design process, in which gear ratios are added as design variables to a structural optimization, has been presented. The integrated process holds the advantage over the sequential approach in that optimization is performed in one continuous run, thereby avoiding the pause and restart required of the sequential process. In addition, it does not require the subjective selection of a trim optimization objective. Demonstration of the process on a lightweight fighter and comparison with a sequential AAW design process have shown that the integrated process holds promise in terms of being able to converge to lower weight solutions than the sequential approach. Future studies will eliminate current limitations associated with the implementation of the integrated process in ASTROS and will examine the effects of different gear ratio starting values on the optimal design.

Acknowledgements

The authors extend thanks to Prof. Moti Karpel and Dr. Boris Moulin of Technion-Israel Institute of Technology for their technical advice and programming assistance.

References

1) Miller, G.D., "Active Flexible Wing (AFW) Technology," Air Force Wright Aeronautical Laboratories, TR-87-3096, February 1988.

2) Perry III, B., Cole, S.R., and Miller, G.D., "A Summary of an AFW Program," Journal of Aircraft, Vol. 32, No. 1.

3) Pendleton, E., Griffin, K., Kehoe, M., and Perry, B., "A Flight Research Program for Active Aeroelastic Wing Technology," 37th AIAA/ASME/ASCE/AHS/ ASC Structures, Structural Dynamics, and Materials Conference, April 1996.

4) Flick, P.M., Love, M.H., and Zink, P.S., "The Impact of Active Aeroelastic Wing Technology on Conceptual Aircraft Design," NATO Research and Technology Agency, Proceedings of the Applied Vehicle Technology Panel Fall 1999 Meeting, Ottawa, Canada, October 1999.

5) Bisplinghoff, R.L., Ashley, H., and Halfman, R.L., Aeroelasticity, Dover Publications, Inc., Mineola, New York, 1955.

6) Miller, G.D., "An Active Flexible Wing Multi-Disciplinary Design Optimization Method," 5th AIAA/USAF/NASA/ISSMO Symposium on Multidisciplinary Analysis and Optimization, Panama City, FL, September 7-9, 1994, AIAA-94-4412.

7) Volk, J. and Ausman, J., "Integration of a Generic Flight Control System into ASTROS," 37th AIAA/ASME/ASCE/AHS/ASC Structures, Structural Dynamics, and Materials Conference, Salt Lake City, UT, April 15-17, 1996, AIAA-96-1335.

8) Ausman, J., and Volk, J., "Integration of Control Surface Load Limiting into ASTROS," 38th AIAA/ ASME/ASCE/AHS/ASC Structures, Structural Dynamics, and Materials Conference, Kissimmee, FL, April 7-10, 1997, AIAA-97-1115.

9) Love, M.H., Barker, D.K., Egle, D.D., Neill, D.J., and Kolonay, R.M., "Enhanced Maneuver Airloads Simulation for the Automated Structural Optimization System – ASTROS," 38th AIAA/ ASME/ ASCE/ AHS/ ASC Structures, Structural Dynamics, and Materials Conference, Kissimmee, FL, April 7-10, 1997.

10) Zink, P.S., Mavris, D.N., and Raveh, D.E., "Maneuver Trim Optimization Techniques for Active Aeroelastic Wings," AIAA/ASME/ASCE/AHS/ASC Structures, Structural Dynamics, and Materials Conference, Atlanta, GA, April 3-6, 2000.

11) Zillmer, S., "Integrated Multidisciplinary Optimization for Active Aeroelastic Wing Design," Air Force Wright Aeronautical Laboratories, WL-TR-97-3087, August 1997.

12) Dobbs, S.K., Schwanz, R.C., and Abdi, F., "Automated Structural Analysis Process at Rockwell," Integrated Airframe Design Technology, Presented at 82nd Meeting of the AGARD Structures and Materials Panel, Sesimbra, Portugal, May 8-9, 1996, AGARD Report 814.

13) Rodden, W.P., and Johnson, E.H., MSC/NASTRAN Version 68 Aeroelastic Analysis User's Guide, The Macneal-Schwendler Corporation, 1994.

14) Neill, D.J., Johnson, E.H., and Canfield, R., "ASTROS-A Multidisciplinary Automated Design Tool," Journal of Aircraft, Vol. 27, No. 12, 1990, pp. 1021-1027.

15) Zink, P.S., Mavris, D.N., Flick, P.M., and Love, M.H., "Impact of Active Aeroelastic Wing Technology on Wing Geometry using Response Surface Methodology," CEAS/AIAA/ICASE/NASA Langley

International Forum on Aeroelasticity and Structural Dynamics, Williamsburg, VA, June 22-25, 1999.

16) Zink, P.S., Mavris, D.N., Flick, P.M., and Love, M.H., "Development of Wing Structural Weight Equation for Active Aeroelastic Wing Technology," SAE/AIAA World Aviation Congress and Exposition, San Francisco, CA, October 19-21, 1999. SAE-1999-01-5640.

17) Dantzig, G.B., Orden, A., Wolfe, P., "The Generalized Simplex Method for Minimizing a Linear Form under Linear Inequality Restraints," Pacific Journal of Mathematics, Vol. 5, 1955, pp. 183 – 195.

18) Karpel, M., Moulin, B., and Love, M.H., "Modal-Based Structural Optimization with Static Aeroelastic and Stress Constraints," Journal of Aircraft, Vol. 34, No. 3, 1997, pp.433-440.

19) Karpel, M., "Modal-Based Enhancement of Integrated Design Optimization Schemes," Journal of Aircraft, Vol. 35, No. 3, 1998, pp. 437-444.

20) Vanderplaats, G.N., and Moses, F., "Structural Optimization by Methods of Feasible Directions," Journal of Computers and Structures, Vol. 3, July 1973, pp. 739-755.

21) Karpel, M., "Modal-Based Structural Optimization using ASTROS-Theoretical Manual," Technion-Israel Institute of Technology, Haifa, Israel, September 1997, TAE No. 795 (Supported by Lockheed Martin Tactical Aircraft Systems, Ft. Worth, TX).

22) Johnson, E.H., and Venkayya, V.B., ASTROS Theoretical Manual, AFWAL-TR-88-3028, December 1988.

23) Rodden, W.P., and Love, J.R., "Equations of Motion of Quasisteady Flight Vehicle Utilizing Restrained Static Aeroelastic Characteristics," Journal of Aircraft, Vol. 22, No. 9, September 1995, pp. 802–809.

24) MathWorks, Inc., Using MATLAB – Version 5, 1996.

25) Zink, P.S., Mavris, D.N., Love, M.H., and Karpel, M., "Robust Design for Aeroelastically Tailored/Active Aeroelastic Wing," 7th AIAA/USAF/NASA/ISSMO Symposium on Multidisciplinary Analysis and Optimization, St. Louis, MO, September 2-4, 1998, AIAA-98-4781.

26) Carmichael, R.L., Castellano, C.R., and Chen, C.F., The Use of Finite Element Methods for Predicting the Aerodynamics of Wing-Body Combinations, NASA SP-228, October 1969.

27) Barker, D.K. and Love, M.H., "An ASTROS Application with Path Dependent Results," AIAA/USAF/NASA/ISSMO Multidisciplinary Analysis and Optimization Conference, Bellevue, WA, September 1996.